JOURNAL OF SPACECRAFT AND ROCKETS
Vol. 33, No. 4, July–August 1996

# Slosh Dynamics Coupled with Spacecraft Attitude Dynamics Part 1: Formulation and Theory

R. J. Hung,* Y. T. Long,† and Y. M. Chi‡
*University of Alabama in Huntsville, Huntsville, Alabama 35899*

**Coupling of slosh dynamics within a partially filled rotating Dewar of superfluid helium II with spacecraft attitude dynamics is investigated in response to the environmental disturbances. These disturbances include 1) lateral impulse, 2) gravity gradient, and 3) *g*-jitter forces. The purpose of this study is to investigate 1) how helium II fluid slosh dynamics driven by various cases of environmental forces coupled with spacecraft dynamics can affect the bubble deformations and their associated fluid and spacecraft mass-center fluctuations and 2) how spacecraft translational displacement, velocity, and accelerations deviating from normal spacecraft operation are induced by the coupling with slosh dynamics driven by various environmental disturbances. The numerical computation of slosh dynamics is based on the rotating frame, whereas the spacecraft dynamics is associated with the nonrotating frame. The results show that major contributions to the orbital dynamics are driven by the coupling with slosh dynamics. Not considering the effect of slosh dynamics acting on the spacecraft may lead to the wrong results for the development of orbital and attitude control techniques.**

## Nomenclature

| | |
|---|---|
| $A$ | = matrix defined in Eq. (12) |
| $\boldsymbol{a}_{gg}$ | = gravity gradient vector, $(a_{gg,r}, a_{gg,\theta}, a_{gg,z})$ in cylindrical coordinates |
| $\boldsymbol{d}$ | = vector (not a unit vector) from the fluid element to the spacecraft mass center |
| $F_x, F_y, F_z$ | = components of forces in Cartesian coordinates |
| $f$ | = *g*-jitter frequency, Hz |
| $g$ | = gravitational acceleration |
| $g_B$ | = background gravity environment |
| $g_0$ | = Earth gravity acceleration, 9.81 m/s$^2$ |
| $h$ | = spacecraft orbit altitude, 650 km for Gravity Probe-B (GP-B) |
| $\boldsymbol{I}$ | = spacecraft moment-of-inertia tensor |
| $M_x, M_y, M_z$ | = components of moments in Cartesian coordinates |
| $m$ | = mass of spacecraft |
| $n$ | = orbital rate of spacecraft, $1.07 \times 10^{-3}$ rad/s for GP-B |
| $R$ | = radius of container |
| $R_c$ | = radius of spacecraft circular orbit, $R_E + h$, 7023 km for GP-B |
| $R_E$ | = radius of the Earth, 6373 km |
| $\boldsymbol{r}_c$ | = unit vector from the spacecraft mass center toward the center of the Earth |
| $(r, \theta, z)$ | = axes in cylindrical coordinate |
| $t$ | = time, s |
| $u, v, w$ | = velocity components in cylindrical coordinates, cm/s |
| $X, Y, Z$ | = inertial-frame Cartesian coordinates for spacecraft dynamics computation |
| $x, y, z$ | = noninertial-frame Cartesian coordinates for fluid dynamics computation |
| $\mu$ | = viscous coefficient of fluid |
| $\rho$ | = density of fluid |
| $\sigma$ | = surface tension coefficient |
| $\tau_0$ | = orbital period of spacecraft, 97.6 min for GP-B |
| $\psi, \theta, \phi$ | = Eulerian angles for heading, attitude, bank |
| $\psi_E$ | = azimuth angle of the Earth with respect to the spacecraft mass center |
| $\omega$ | = angular velocity of spacecraft spinning along the $z$ axis |

*Subscripts*

| | |
|---|---|
| $c$ | = spacecraft mass center |
| $D$ | = residual environmental components |
| $L$ | = fluid slosh components |
| $X, Y, Z$ | = inertial-frame components along the $X, Y, Z$ directions |
| $x, y, z$ | = noninertial-frame components along the $x, y, z$ directions |
| $\psi, \theta, \phi$ | = rotational components along the $\psi, \theta, \phi$ directions |

## Introduction

TO carry out scientific experiments, some experimental spacecraft use cryogenic cooling for telescope instrumentation, use superconducting sensors for gyro readout, and maintain temperatures near absolute zero for mechanical stability. The approaches to both cooling and control involve the use of helium II. In this study, coupling of spacecraft attitude dynamics with sloshing dynamics driven by orbit environmental disturbances is investigated. Fluid management problems may arise from an asymmetric distribution of helium liquid and vapor due to perturbations in the liquid–vapor interface. A basic understanding of slosh dynamics coupled with orbital dynamics in six degrees of freedom is important in the development of spacecraft guidance and attitude control systems.

Liquid helium at a temperature of 1.8 K is used as the coolant. Because it is a superfluid, there are at most only very small temperature gradients in the liquid helium. In the absence of Marangoni convection, in view of the negligibly small temperature dependence of surface tension and negligible thermal gradients along the liquid–vapor interface, the equilibrium shape of the interface is governed by a balance of capillary, centrifugal, gravitational,[1–3] and dynamical forces. Determination of the liquid–vapor interface profile based on computational experiments can uncover details of the flow that cannot be easily visualized or measured experimentally in a microgravity environment.[1–3]

Instability of the liquid–vapor interface can be induced by the presence of longitudinal and lateral accelerations. Thus, slosh waves

Received May 15, 1995; revision received March 9, 1996; accepted for publication March 18, 1996. 

*Professor, Mechanical and Aerospace Engineering. Associate Fellow AIAA.

†Senior Research Scientist, Department of Mechanical and Aerospace Engineering.

‡Research Assistant, Department of Mechanical and Aerospace Engineering.

are excited, producing high- and low-frequency oscillations in the liquid helium. The sources of the residual accelerations include effects of the Earth's gravity gradient[1-3] and $g$-jitter.[4-6] A recent study suggests that the high-frequency accelerations may be unimportant in comparison with the residual motions caused by low-frequency accelerations.[4]

The time-dependent behavior of liquid helium in a partially filled rotating Dewar in reduced-gravity environments is simulated by numerically solving the Navier–Stokes equations subject to initial and boundary conditions.[5,6] At the interface between the liquid and the vapor fluids, both the kinematic surface boundary condition and the interface stress conditions for components tangential and normal to the interface are applied.[5,6] The initial conditions are adopted from the steady-state formulations.[7] Some of the steady-state formulations of interface shapes are compared with available experiments[8] in a free-falling aircraft (KC-135). The experiments[9] show that the classical fluid mechanics theory is applicable to cryogenic helium in large containers with velocities greater than the corresponding critical velocities.[10-13]

At temperatures close to absolute zero, quantum effects begin to be of importance in the properties of superfluids. At a temperature of 2.17 K, liquid helium undergoes a second-order phase transition; at temperatures below this point, liquid helium (helium II) has a number of remarkable properties, the most important of which is superfluidity. This property permits flow without viscosity in narrow capillaries or gaps. At temperatures other than zero, helium II behaves as if it were a mixture of two different liquids. One of these is a superfluid and moves with zero viscosity along a solid surface. The other is a normal viscous fluid. The two motions occur without any transfer of momentum from one to another for velocities below a critical velocity.[10-12] Above the critical velocity, the two fluids are coupled through their mutual friction.[10-15]

The key parameters affecting the critical velocity are temperature and container size. To determine the dynamical behavior of helium II in a large rotating cylinder, the mutual friction of the two fluid components is allowed for in the model computation. The density of the superfluid is a function of temperature, as are the surface tension and viscous coefficient for helium II.[10-17] In this study, the theory of viscous Newtonian fluids is employed with temperature-dependent transport coefficients.

Transient phenomena due to slosh reaction torques driven by three types of environmental accelerations coupled with spacecraft orbital dynamics are investigated. Mathematical formulations of 1) slosh dynamics based on fluid dynamics and 2) attitude dynamics based on translational and rotational formulations of spacecraft dynamics have been numerically solved simultaneously.

Three types of environmental forces are considered in this study: 1) lateral impulse, 2) gravity gradient, and 3) $g$-jitter acceleration. Coupling between slosh dynamics and orbital dynamics will cause the behavior of the bubble to differ significantly from that driven by slosh dynamics alone. The deformation of the bubble is quite different from the results obtained earlier[15,18] without taking account of the modification of orbital dynamics. Furthermore, attitude dynamics driven by slosh dynamics can cause the spacecraft to deviate from normal operation.[19]

## Noninertial-Frame Mathematical Formulation of Slosh Dynamics

An experiment made by Andronikashvili[10-13] on rotating helium II shows that it is necessary to exceed a critical velocity for the interaction between the normal and superfluid components to set an entire bucket in rotation.[10-13] For a rotating Dewar with o.d. 1.56 m and i.d. 0.276 m, the critical velocities are $6.4 \times 10^{-7}$ and $3.6 \times 10^{-6}$ m/s, respectively.[10-15] With a rotational speed of 0.1 rpm, the linear velocities along the outer and inner walls of the rotating Dewar are $8.17 \times 10^{-3}$ and $1.45 \times 10^{-3}$ m/s, respectively, which are at least several hundred times greater than the corresponding critical velocities. From this illustration it is seen that the problem under consideration has special features that warrant the adoption of a model with viscous Newtonian fluids in this study.

Consider a closed circular Dewar partially filled with helium II. The whole fluid system is spinning about the axial direction $z$ of cylindrical coordinates $r$, $\theta$, $z$, with corresponding velocity components $u$, $v$, $w$. The governing equations for noninertial-frame spacecraft-bound coordinates spinning about the $z$ axis have been given in our recent studies.[20-22] Dynamical forces, such as gravity gradient, $g$-jitter, and angular accelerations, as well as centrifugal, Coriolis, surface tension, viscous forces, etc., are given explicitly in the mathematical formulations.[18-24] In the computation of sloshing reaction forces, moments, viscous stresses, and angular momenta acting on the container wall of the spacecraft, one must consider those forces and moments in the inertial frame rather than in the noninertial frame.[20-24]

For solving slosh-dynamic problems of liquid systems in orbital spacecraft under a microgravity environment, one must solve the governing equations[21,23] accompanied by a set of initial and boundary conditions. A detailed illustration of these initial and boundary conditions for the slosh dynamics of fluid systems in microgravity has been given by Hung and Pan.[19-22,24] The computational algorithms applicable to cryogenic fluid management under microgravity have also been given earlier.[20-24] Computational algorithms are summarized in Fig. 1. In this study, to show a realistic example, a Dewar with an outer radius of 0.78 m and an inner radius of 0.138 m, top and bottom radii of 1.10 m, and a height of 1.62 m has been used in the numerical simulation. The Dewar tank is 80% filled with liquid helium, and the ullage is filled with helium vapor (the total fluid mass is 287.6 kg). The temperature of the liquid helium is 1.8 K. In this study the following data are used: liquid helium density 145.7 kg/m$^3$, helium vapor density 0.45 kg/m$^3$, fluid pressure 1.6625 Pa, surface tension coefficient at the interface between liquid helium and helium vapor 0.0353 N/m, liquid helium viscosity coefficient $9.61 \times 10^{-9}$m$^2$/s, and contact angle 0 deg. The initial profiles

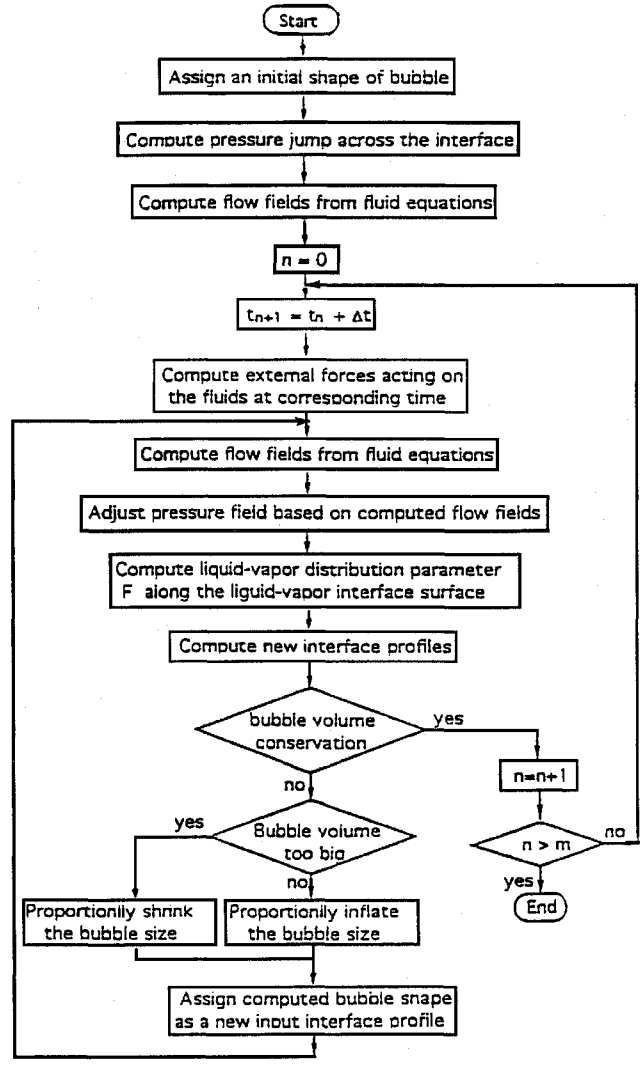


**Fig. 1 Computational algorithm for sloshing dynamics.**

of the liquid–vapor interface for the rotating Dewar are determined from computations based on algorithms developed for the steady-state formulation of microgravity fluid management.[7,25]

A staggered grid for the velocity components is used in this computer program. The marker-and-cell method[26] of studying fluid flows along a free surface is adopted. The volume of fluid method is used to solve finite difference equations numerically. The approximate flow velocity is calculated from the explicit approximation of momentum equations based on the results from the previous time step. Computation of pressure and velocity at the new time step are thus obtained from iteratively solving the pressure equation with the conjugate residual technique.[27–30] The configuration of the liquid–vapor interface adjusted for the surface tension effect at the new time step is then finally obtained. The time step during this computation is automatically adjusted through the fulfillment of the stability criteria for the computed grid size. The convergence criterion for the iteration of the pressure equation is based on the computed velocity at each cell, which satisfies the continuity equation with errors no more than $10^{-5}$ of the velocity difference.[31] For the volume conservation of liquid, a deviation of less than 1% in volume is always required before a move to the next time step.

In this study, characteristics of the slosh reaction force and torque fluctuations exerted on the Dewar in response to various accelerations of the spacecraft are also investigated. The mathematical formulation of the fluctuations of slosh reaction forces and torques exerted on the Dewar is given elsewhere.[21,32,33] With reference to slosh dynamics driven by impulse[15,18] and environmental disturbances[14,19,20] with their mathematical formulations,[21,32,33] one can calculate the slosh reaction force and associated torque acting on the Dewar. These quantities are required for the computation of the coupling between the slosh dynamics of helium II and the attitude dynamics.

## Inertial-Frame Mathematical Formulation of Spacecraft Dynamics

In spacecraft dynamics, a rigid body with six degrees of freedom, three being translational and three rotational, is considered. In this study, our primary interest is to investigate the slosh reaction torques driven by 1) lateral impulse, 2) gravity-gradient-dominated, and 3) $g$-jitter-dominated accelerations coupled with spacecraft dynamics. In other words, our main purpose is to investigate how the slosh reaction forces and torques coupled with spacecraft dynamics can affect the cryogenic bubble deformations and their associated fluid and spacecraft mass-center fluctuations, and how these effects feed back to the attitude dynamics. General practice in attitude dynamics adopts spring–mass–damper models,[34] which are formulated mathematically as ordinary differential equations. In view of the slosh dynamics displayed by nonlinear bubble oscillations and deformations, which are governed by nonlinear partial differential equations accompanied by nonlinear boundary conditions,[21,22] it is very hard, if not impossible, to describe the physics of slosh dynamics coupled with attitude dynamics in terms of such spring–mass–damper models.[34,35]

The three translational governing equations are given by

$$\frac{\mathrm{d}}{\mathrm{d}t}(m\dot{X}_i) = F_{Di} + F_{Li} \tag{1}$$

where $F_D$ and $F_L$ denote the residual environmental force and the slosh reaction force (from the fluid system) on the spacecraft, respectively.[19,20,30,31] Subscript $i$ denotes the component along direction $i$ (= $X$, $Y$, or $Z$ in the nonrotational frame), and single and double dots ($\dot{X}$, $\ddot{X}$) imply first and second time derivatives of the parameter, respectively. Eulerian angles are defined to accommodate three rotational equations.[35] The three rotational equations in terms of Eulerian angles are given by

$$I_t(\ddot{\theta} + \dot{\psi}^2 \sin\theta\cos\theta) + I_a\dot{\psi}\cos\theta(\dot{\phi} - \dot{\psi}\sin\theta) = M_\theta \tag{2}$$

$$I_a[(-\ddot{\theta} + \ddot{\psi}\sin\theta + \dot{\psi}\dot{\theta}\cos\theta)\sin\theta - \dot{\theta}(\dot{\phi} - \dot{\psi}\sin\theta)\cos\theta] + I_t(\ddot{\psi}\cos^2\theta - 2\dot{\psi}\dot{\theta}\sin\theta\cos\theta) = M_\psi \tag{3}$$

$$I_a(\ddot{\theta} - \ddot{\psi}\sin\theta - \dot{\psi}\dot{\theta}\cos\theta) = M_\phi \tag{4}$$

where

$$M_\theta = (M_{Lx} + M_{Dx})\cos\phi - (M_{Ly} + M_{Dy})\sin\phi \tag{5}$$

$$M_\psi = (M_{Lx} + M_{Dx})\sin\phi\cos\theta + (M_{Ly} + M_{Dy})\cos\phi\cos\theta - (M_{Lz} + M_{Dz})\sin\theta \tag{6}$$

$$M_\phi = (M_{Lz} + M_{Dz}) \tag{7}$$

Here $M_{Li}$ and $M_{Di}$ are the slosh reaction torque acting on the Dewar and the residual torque acting on the spacecraft, respectively, along direction $i$ ($i = x$, $y$, or $z$ in the noninertial frame). $I_a$ (= $I_{zz}$) and $I_t$ (= $I_{xx} = I_{yy}$) denote the moments of inertia about the axial and transverse directions, respectively.

Activation of slosh dynamics in response to lateral impulse and environmental disturbances, such as gravity and $g$-jitter accelerations, coupled with spacecraft dynamics must induce angular velocities $\omega_1$, $\omega_2$, $\omega_3$ along the $x$, $y$, $z$ coordinates in the rotational frame. We can assume that $(\omega_1, \omega_2, \omega_3) = (\dot{\theta}_1, \dot{\theta}_2, \dot{\theta}_3)$, where $\dot{\theta}_1$, $\dot{\theta}_2$, $\dot{\theta}_3$ are the time derivatives of the angular displacements about the $x$, $y$, $z$ coordinates. With the definition of $I_{xx} = I_1$, $I_{yy} = I_2$, and $I_{zz} = I_3$, the spinning angular velocity in the rotational frame can be expressed as follows[35]:

$$\begin{aligned}
\ddot{\theta}_1 + K_1\dot{\theta}_2\dot{\theta}_3 &= (1/I_1)(M_{Lx} + M_{Dx}) \\
\ddot{\theta}_2 + K_2\dot{\theta}_1\dot{\theta}_3 &= (1/I_2)(M_{Ly} + M_{Dy}) \\
\ddot{\theta}_3 + K_3\dot{\theta}_1\dot{\theta}_2 &= (1/I_3)(M_{Lz} + M_{Dz})
\end{aligned} \tag{8}$$

where $K_1 = (I_3 - I_2)/I_1$, $K_2 = (I_1 - I_3)/I_2$, and $K_3 = (I_2 - I_1)/I_3$. Both the translational and rotational equations are initial-value problems. The initial conditions for the translational equations and for the rotational equations are

$$\begin{aligned}
(X, Y, Z) &= (0, 0, 0)\ \text{cm} \\
(\dot{X}, \dot{Y}, \dot{Z}) &= (0, 0, 0)\ \text{cm/s} \qquad \text{at} \quad t = 0
\end{aligned} \tag{9}$$

and

$$\begin{aligned}
(\theta, \psi, \phi) &= (0, 0, 0)\ \text{rad} \\
(\dot{\theta}, \dot{\psi}, \dot{\phi}) &= (0, 0, 0.1)\ \text{rpm} \qquad \text{at} \quad t = 0
\end{aligned} \tag{10}$$

In this paper, a rotating (noninertial) frame is adopted in the study of the slosh dynamics, and a nonrotating (inertial) frame in the study of attitude dynamics. The conversion matrix $A$ is used to make the conversion from the parameters in the nonrotational frame ($X, Y, Z$) to those in the rotating frame ($x, y, z$) through the use of the following mathematical expression:

$$\begin{bmatrix} x \\ y \\ z \end{bmatrix} = A \begin{bmatrix} X \\ Y \\ Z \end{bmatrix} \tag{11}$$

where

$$A = \begin{bmatrix} A_{XX} & A_{XY} & A_{XZ} \\ A_{YX} & A_{YY} & A_{YZ} \\ A_{ZX} & A_{ZY} & A_{ZZ} \end{bmatrix} \tag{12}$$

with

$$\begin{aligned}
A_{XX} &= -\sin\psi\cos\phi + \cos\psi\sin\theta\sin\phi \\
A_{YX} &= \sin\psi\sin\phi + \cos\psi\sin\theta\cos\phi \\
A_{ZX} &= \cos\psi\cos\theta \\
A_{XY} &= \cos\psi\cos\phi + \sin\psi\sin\theta\sin\phi \\
A_{YY} &= -\cos\psi\sin\phi + \sin\psi\sin\theta\cos\phi \\
A_{ZY} &= \sin\psi\cos\theta \\
A_{XZ} &= \cos\theta\sin\phi \\
A_{YZ} &= \cos\theta\cos\phi \\
A_{ZZ} &= -\sin\theta
\end{aligned}$$

**Table 1 Characteristics of various environmental-disturbance-driven sloshing dynamics**

| | Lateral impulse | Gravity-gradient force | $g$-jitter force |
|---|---|---|---|
| Type of force | Spotty $\delta$-function | Continuous spectrum | Continuous spectrum |
| Magnitude of force | $10^{-3}g_0$ | $10^{-7}g_0$ | $10^{-6}g_0$ |
| Time period of force acting | $10^{-2}$s | Full orbit period | Full orbit period |
| Magnitude range of force | $(10^{-2}$–$10^{-9})g_0$ | $10^{-7}g_0$ | $(10^{-5}$–$10^{-9})g_0$ |
| Magnitude of force acting on fluid element at different locations | Same | Different | Same |
| Type of fluid motion | Leftward–rightward oscillations | Tidal mode motion | Leftward–rightward and up–down oscillations |

As $A$ is an orthogonal matrix ($A^{-1} = A^T$), Eq. (11) becomes

$$\begin{bmatrix} X \\ Y \\ Z \end{bmatrix} = A^T \begin{bmatrix} x \\ y \\ z \end{bmatrix} \tag{13}$$

For calculating the coupling of slosh dynamics and spacecraft attitude dynamics, shown in Eqs. (1–4), an iteration method at every time step is adopted to determine $F_{Di}$, $M_{Di}$ for the spacecraft, which are mutually coupled with $F_{Li}$, $M_{Li}$ from the slosh dynamics. The computational algorithm is summarized in Fig. 2, where the superscript $k$ is the iteration number. In this computation, the dry mass of the spacecraft (excluding fluid mass) is assumed to be 350 kg, the fluid mass for 80% liquid filling is 287.6 kg, and the moment of inertia of the spacecraft is $I_{xx} = I_{yy} = 160.3\ \text{kg} \cdot \text{m}^2$ and $I_{zz} = 154.5\ \text{kg} \cdot \text{m}^2$.

## Characteristics of Orbit Environmental Disturbances

The characteristics of the three types of orbital environmental disturbance action on fluid systems considered in this study are quite different. Lateral impulse is in the form of a spotty $\delta$ function with a short time period of $10^{-2}$ s, whereas both the gravity gradient and $g$-jitter forces are in the form of continuous spectra covering whole spacecraft orbital periods. The magnitudes of these accelerations vary from $10^{-2}$ to $10^{-9}g_0$, and they act on fluid elements at different locations with different magnitudes in the case of gravity gradient forces and with the same magnitude in the case of impulse and $g$-jitter forces. They are described in Table 1.

It is assumed that a lateral impulse with the following forms of force $F_i$ and torque $M_i$ act on the spacecraft system in the noninertial (rotating) frame (in Cartesian coordinates)[15,18]:

$$\begin{aligned} F_i &= (F_x, F_y, F_z) = (20, 0, 0)\ \text{N} \\ M_i &= (M_x, M_y, M_z) = (0, 10, 0)\ \text{N} \cdot \text{m} \end{aligned} \tag{14}$$

for $0 \le t \le 10^{-2}$s and

$$\begin{aligned} F_i &= (0, 0, 0)\ \text{N} \\ M_i &= (0, 0, 0)\ \text{N} \cdot \text{m} \end{aligned} \tag{15}$$

for $t > 10^{-2}$s. With a spacecraft mass of 637.6 kg, the lateral impulse is equivalent to $3.2 \times 10^{-3}g_0$ in this case. In general, lateral impulses range in magnitude from $10^{-2}$ to $10^{-9}g_0$.

To give an example, for the Gravity Probe-B (GP-B) spacecraft, which is an Earth satellite orbiting at 650-km altitude directly over the poles, the orbital period $\tau_0$ can be computed from the following expression[2]:

$$\tau_0 = 2\pi \frac{R_c^{\frac{3}{2}}}{R_E g_0^{\frac{1}{2}}} \tag{16}$$

For the case of GP-B, the orbital period $\tau_0 = 97.6$ min (5856 s) and the orbital rate $n = 2\pi/\tau_0 = 1.07 \times 10^{-3}$ rad/s.

The gravity gradient acceleration acting on the fluid mass of spacecraft can be shown to be[1–3,19–22]

$$\boldsymbol{a}_{gg} = -n^2[3(\boldsymbol{r}_c \cdot \boldsymbol{d})\boldsymbol{r}_c - \boldsymbol{d}] \tag{17}$$

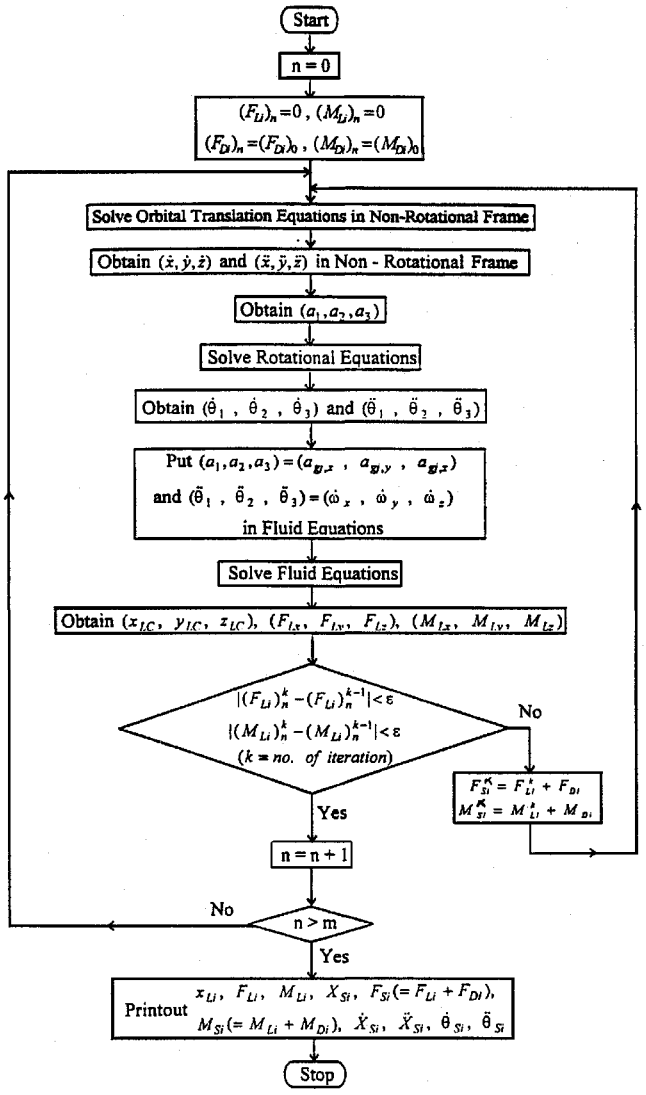


**Fig. 2 Computational algorithm for coupling of sloshing and orbital dynamics.**

In the case of the GP-B spacecraft, it is assumed that the gravity gradient[1–3] exerted on the mass center (balanced by the centrifugal forces of the orbiting spacecraft) is zero when the spacecraft is orbiting the Earth on its specified orbit. In other words, all the gravity acceleration exerted on the spacecraft is the gravity gradient acceleration[1–3] as defined in Eq. (17). Figure 3A illustrates the geometrical relationship of the parameters shown in Eq. (17).

At time $t = 0$, the rotating axis of the spacecraft is aligned with the radial direction from the Earth's center to the spacecraft mass's center. The azimuth angle of Earth with respect to the spacecraft mass center, $\psi_E$, can be computed from the orbital period obtained from Eq. (16) for the normal operation of the spacecraft:

$$\psi_E = 2(\pi/\tau_0)t \tag{18}$$

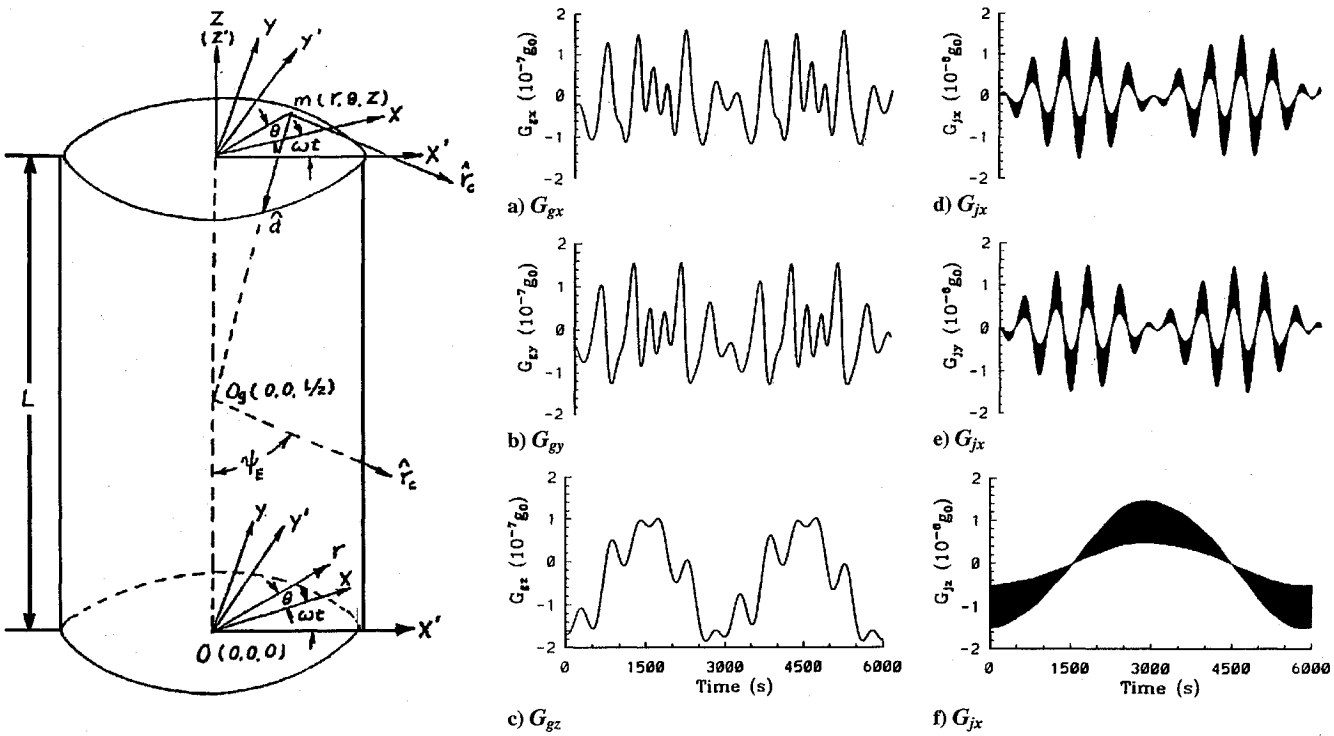


**A) Geometry of gravity gradient acceleration**

**B) Time variation of gravity gradient acceleration**

**C) Time variation of $g$-jitter acceleration**

**Fig. 3 Time evolution of gravity gradient and $g$-jitter accelerations acting on the spacecraft during a full orbit period.**

where $t$ is the time measured from the instant when the spacecraft spin axis is aligned with the radial direction from the spacecraft mass center to the center of the Earth. Some modification is required if coupling of slosh and orbital dynamics, leading to deviation of the spacecraft orbit from normal operation, is considered.

Fluctuations of residual gravity due to $g$-jitter acceleration are modeled by the following equation[18–20]:

$$g = g_B\left[1 + \tfrac{1}{2}\sin(2\pi f t)\right] \tag{19}$$

In this study, $g$-jitter acceleration with background gravity of $10^{-8}g_0$ due to spacecraft atmospheric drag, in an example with rotational speed of 0.1 rpm for normal GP-B spacecraft operation, and three frequencies of $g$-jitter with the values 0.1, 1.0, and 10 Hz have been considered[4] for the investigation of the oscillations of the liquid–vapor interface. The components of the $g$-jitter acceleration in the noninertial coordinate system are given by[18–20]

$$\hat{a}_{gj} = (a_{gj,r}, a_{gj,\theta}, a_{gj,z}) = [g\sin\psi_E\cos(\theta + \omega t),$$
$$-g\sin\psi_E\sin(\theta + \omega t), -g\cos\psi_E] \tag{20}$$

The characteristics of gravity gradient and jitter accelerations shown in Eqs. (17) and (20), respectively, are quite different. Gravity gradient acceleration has the following two characteristics:

1) The acceleration acting on any fluid mass inside the container increases quadratically in the component of the distance from the mass center of the container (point $O_g$ in Fig. 3A) to the location of the fluid mass parallel to the line from the mass center of the container to the center of the Earth (parallel to unit vector $\boldsymbol{r}_c$ shown in Fig. 3A).

2) The acceleration acting on the fluid mass decreases linearly in the shortest distance from the location of the fluid mass to the radius along the vector from the mass center of the container to the center of the Earth.[17–19]

To give an example, Fig. 3B shows the time variation of gravity gradient accelerations for a full orbit period of 5856 s with container rotating speed 0.1 rpm for components along the $x$, $y$, $z$ directions acting on the fluid mass located at ($r$, $\theta$, $z$) = (40 cm, $\pi/4$, 10 cm). Because the magnitude and direction of gravity gradient acceleration acting on each fluid mass are strongly dependent on how far the location of the fluid mass deviates from the mass center of the container measured along the axis parallel to the vector $\boldsymbol{r}_c$, which varies with respect to time, we see that the gravity gradient acceleration acting on a fluid mass is different for fluid masses at different locations in the container. There is a symmetry between the two half orbital periods in the time evolution of gravity gradient acceleration if the ratio of orbital period to spacecraft spin period is an integer and the spacecraft is in normal operation.[18–20] However, coupling of slosh and orbital dynamics, as shown in Fig. 3B, leads to asymmetry in the time evolution of gravity gradient acceleration.[18–20] Figure 3B also shows that the magnitude of gravity gradient accelerations[1–3] is on the order of $10^{-7}g_0$.

Contrary to gravity gradient acceleration,[1–3] $g$-jitter acceleration drives the same acceleration of the fluid mass at all locations in the container. Figure 3C shows the time variation of $g$-jitter accelerations for a full orbital period of 5856 s with a container rotational speed of 0.1 rpm and a jitter frequency of 0.1 Hz for components along the $x$, $y$, $z$ directions. Again, symmetry is shown between half orbital periods of the time evolution of the acceleration if the ratio of orbital period to spacecraft spin period is an integer and the spacecraft is in normal operation.[18–20] Coupling of slosh and orbital dynamics as shown in Fig. 3C again leads to asymmetry.[18–20] In general, $g$-jitter acceleration ranges in magnitude from $10^{-5}$ to $10^{-9}g_0$. With background gravity of $10^{-6}g_0$ for the $g$-jitter acceleration considered in this study, the combined gravity gradient (on the order of $10^{-7}g_0$) and $g$-jitter accelerations acting on the spacecraft correspond to the case of orbital accelerations dominated by $g$-jitter forces acting on fluid system of the spacecraft.

## Similarity Considerations

The present study considers the dynamic behavior of superfluid helium II. As mentioned earlier, the rotational velocities of helium II considered in this study are much greater than the critical velocities,[9–14] so that the adoption of a Newtonian fluid formulation is warranted. In other words, the formulation considered in this study is completely identical to that for conventional fluids such as liquid nitrogen, liquid hydrogen, or hydrazine. To deal with conventional fluids with various physical properties, similarity considerations of nondimensionalized parameters, such as Bond number,

capillary number, Weber number, Reynolds number, etc., should be considered in the mathematical formulation. Detailed discussions of the mathematical formulations and physical interpretations of similarity rules have been given precisely by Hung et al.,[6] and a brief discussion will be presented in this paper.

Similarity rules are used to compare the results of a slosh-dynamic computation with different sizes of Dewar, different liquid-filled levels, and different working fluids inside the Dewar considered.[6] Obviously, the slosh effect vanishes when the liquid fill level is at an extreme of 100% (fully filled) and 0% (completely empty). The slosh effect becomes dominant for liquid fill levels in the range of 40–60%, depending on the characteristics of the nonlinear effects of environmental disturbances. Characteristics of various working fluids are controlled by their transport properties, such as density, viscosity, surface tension, and specific heat. These material properties, along with the dynamical parameters such as velocity, acceleration, rotational speed, and geometry of container, can be combined and formed into various sets of dimensionless parameters based on the similarity rules.[6] In other words, characteristics of fluid flows associated with slosh dynamics are controlled by material properties together with dynamics and geometrical parameters, such as environmental disturbances (including impulse, gravity gradient, and $g$-jitter acceleration), surface tension, viscous forces, centrifugal forces, container size, etc. These parameters can be combined into the following similarity factors:

$$B_0 = \frac{\rho g R^2}{\sigma} = \frac{\text{gravity force}}{\text{surface tension force}} \tag{21}$$

$$C_a = \frac{\mu R \omega}{\sigma} = \frac{\text{viscous force}}{\text{surface tension force}} \tag{22}$$

$$W_e = \frac{\rho \omega^2 R^3}{\sigma} = \frac{\text{centrifugal force}}{\text{surface tension force}} \tag{23}$$

$$R_e = \frac{\rho \omega R^2}{\mu} = \frac{\text{centrifugal force}}{\text{viscous force}} \tag{24}$$

where $B_0$, $C_a$, $W_e$, and $R_e$ denote the Bond number, dynamical capillary number, Weber number, and rotational Reynolds number, respectively. Note that the capillary number is the ratio of the Weber number to the Reynolds number.

For the cases of flows with various working fluids, such as liquid helium, liquid hydrogen, liquid nitrogen, and hydrazine, $\rho$, $\mu$, and $\sigma$ are the material constants, whereas $\omega$, $g$, and $R$ (the rotational speed, the gravity environment, and the size of the Dewar, respectively) are the dynamical and geometrical parameters, which are adjustable in computer experiments. Hung et al.[6] indicate that the Bond number, dynamical capillary number, Weber number, and rotational Reynolds number determine the wave period, wave-induced slosh reaction force, wave amplitude, and flow profile, respectively, for slosh-wave excitation along the liquid–vapor interface by orbital acceleration. Because $B_0$, $C_a$, $W_e$, and $R_e$ are functions of $gR^2$, $R\omega$, $\omega^2 R^3$, and $\omega R^2$, respectively, the proper adjustment of the combinations of $g$, $R$, and $\omega$ can better correlate the relationship among various sizes and shapes and different amplitudes of orbital acceleration through the employment of the scaling of similarity rules presented by Hung et al.[6]

By using the similarity rules considered in this section, various working fluids (such as liquid helium, liquid nitrogen, liquid hydrogen, and hydrazine) with different sizes of Dewar, various amplitudes of environmental disturbances, etc., can be covered in the models presented in this study.

The discussions in this study are basically applicable to conventional Newtonian fluids. However, the computational model presented is also applicable to non-Newtonian fluids with proper modification. In particular, the models of slosh reaction forces and torques employed in this study are also applicable provided that the proper adjustment is given to the definition of viscosity $\mu$ based on the ratio of viscous stress $\tau$ to fluid velocity shear $\partial u/\partial y$, i.e.,

$$\mu = \frac{\tau}{(\partial u/\partial y)^n} \tag{25}$$

where $n = 1$ for Newtonian fluids and $n \neq 1$ for non-Newtonian fluids. Here $u$, $y$, and $n$ denote the fluid velocity, coordinate transverse to the fluid velocity, and numerical proportionality parameter, respectively. Thus the mathematical formulations presented in this paper are quite general and cover the coupling of slosh and spacecraft attitude dynamics, which includes both Newtonian and non-Newtonian fluids, with proper modifications.

Application of the formulation and theory to realistic orbital environment disturbances will be fully illustrated in Part 2 of this paper.[36]

## Conclusion

A mathematical formulation and theory for the slosh dynamics of fluid motions coupled with spacecraft attitude dynamics have been presented. The dynamics of a spacecraft Dewar activated by environmental disturbances including 1) lateral impulse, 2) gravity gradient, and 3) $g$-jitter accelerations have been illustrated. A mathematical algorithm for calculating the coupling between helium II slosh dynamics and attitude dynamics has been discussed and illustrated, which can find the slosh reaction forces and torques coupled with translational and rotational dynamics of spacecraft, as a result of deviation of the spacecraft from normal operation.

For the purpose of the study, the slosh dynamics is based on a rotating frame, and the attitude dynamics on a nonrotating frame. Among the three environmental disturbances acting on the spacecraft chosen in this study, both the gravity-gradient and $g$-jitter forces are in the form of continuous spectra, whereas the lateral impulse is in the form of a spotty $\delta$ function. All of these forces are capable of exciting slosh dynamics coupled with attitude dynamics. The asymmetric orientation of the helium II liquid sloshing in the tank, driven by the three kinds of forces considered, may also create control and pointing problems.

## Acknowledgments

The authors appreciate the support received from NASA through Grant NAG8-938 and Contract NAS839609/Delivery Order 103.

## References

[1]Avduyevsky, V. S. (ed.), *Scientific Foundations of Space Manufacturing*, MIR, Moscow, 1984, p. 450.

[2]Forward, R. L., "Flattening Space-Time Near the Earth," *Physical Review A*, Vol. 26, No. 5, 1982, pp. 735–744.

[3]Misner, C. W., Thorne, K. S., and Wheeler, J. A., *Gravitation*, Freeman, San Francisco, 1973, pp. 253–674.

[4]Kamotani, Y., Prasad, A., and Ostrach, S., "Thermal Convection in an Enclosure Due to Vibrations Aboard a Spacecraft," *AIAA Journal*, Vol. 19, No. 4, 1981, pp. 511–516.

[5]Hung, R. J., Lee, C. C., and Leslie, F. W., "Spacecraft Dynamical Distribution of Fluid Stresses Activated by Gravity Jitters Induced Slosh Waves," *Journal of Guidance, Control, and Dynamics*, Vol. 15, No. 3, 1992, pp. 817–824.

[6]Hung, R. J., Lee, C.C., and Leslie, F. W., "Similarity Rules in Gravity Jitter-Related Spacecraft Liquid Propellant Slosh Waves Excitation," *Journal of Fluids and Structures*, Vol. 6, No. 3, 1992, pp. 493–522.

[7]Hung, R. J., Tsao, Y. D., Hong, B. B., and Leslie, F. W., "Bubble Behaviors in a Slowly Rotating Helium Dewar in Gravity Probe-B Spacecraft Experiment," *Journal of Spacecraft and Rockets*, Vol. 26, No. 1, 1989, pp. 167–172.

[8]Leslie, F. W., "Measurements of Rotating Bubble Shapes in a Low Gravity Environment," *Journal of Fluid Mechanics*, Vol. 161, No. 2, 1985, pp. 269–279.

[9]Mason, P., Collins, D., Petrac, D., Yang, L., Edeskuty, F., Schuch, A., and Williamson, K., "The Behavior of Superfluid Helium in Zero Gravity," *Proceedings of the 7th International Cryogenic Engineering Conference* (Surrey, England, UK), Science and Technology Press, 1978, pp. 101–114.

[10]Donnelly, R. J., "Superfluid Turbulence," *Scientific American*, Nov. 1988, pp. 100–122.

[11]Van Sciver, S. W., *Helium Cryogenics*, Plenum, New York, 1986, p. 429.

[12]Donnelly, R. J., *Quantized Vortices in Helium II*, Cambridge Univ. Press, Cambridge, England, UK, 1991, p. 384.

[13]Wilks, J., and Betts, D. S., *An Introduction to Liquid Helium*, Clarendon, Oxford, England, UK, 1987, p. 187.

[14]Hung, R.J., Pan, H. L., and Long, Y. T., "Peculiar Behavior of Helium II Disturbances Due to Sloshing Dynamics Driven by Jitter Accelerations Associated with Slew Motion in Microgravity," *Cryogenics*, Vol. 34, No. 8, 1994, pp. 641–648.

[15]Hung, R. J., and Long, Y. T., "Effect of Baffle on Slosh Reaction Forces in Rotating Liquid Helium Subjected to a Lateral Impulse in Microgravity," *Cryogenics*, Vol. 35, No. 9, 1995, pp. 589–597.

[16]Wilks, H., *The Properties of Liquid and Solid Helium*, Clarendon, Oxford, England, UK, 1967.

[17]Hoare, F. E., Jackson, L. C., and Kurti, N., *Experimental Cryogenics: Liquid Helium II*, Butterworths, London, 1961.

[18]Hung, R. J., and Long, Y. T., "Response and Decay of the Rotating Cryogenic Liquid Reacted to Impulsive Accelerations in Microgravity," *Transaction of the Japan Society for Aeronautical and Space Science*, Vol. 37, No. 2, 1995, pp. 291–310.

[19]Hung, R.J., and Pan, H. L., "Fluid Force Activated Spacecraft Dynamics Driven by Gravity Gradient and Jitter Accelerations," *Journal of Guidance, Control, and Dynamics*, Vol. 18, No. 5, 1995, pp. 1190–1196.

[20]Hung, R. J., and Pan, H. L., "Differences in Gravity Gradient and Gravity Jitter Excited Slosh Waves in Microgravity," *Transaction of the Japan Society for Aeronautical and Space Sciences*, Vol. 36, No. 1, 1993, pp. 153–169.

[21]Hung, R. J., and Pan, H. L., "Gravity Gradient or Gravity Jitter Induced Viscous Stress and Moment Fluctuations in Microgravity," *Fluid Dynamic Research*, Vol. 34, No. 1, 1994, pp. 29–44.

[22]Hung, R. J., and Pan, H. L., "Mathematical Model of Bubble Sloshing Dynamics for Cryogenics Liquid Helium in Orbital Spacecraft Dewar Container," *Applied Mathematics Modeling*, Vol. 19, No. 8, 1995, pp. 483–498.

[23]Hung, R. J., Pan, H. L., and Leslie, F. W., "Fluid System Angular Momentum and Moment Fluctuations Gravity Gradient of Gravity Jitter in Microgravity," *Journal of Flight Sciences and Space Research*, Vol. 18, No. 1, 1994, pp. 195–202.

[24]Hung, R. J., and Pan, H. L., "Asymmetric Slosh Wave Excitation in Liquid–Vapor Interface Under Microgravity," *Acta Mechanica Sinica*, Vol. 9, No. 2, 1993, pp. 298–311.

[25]Hung, R. J., and Leslie, F. W., "Bubble Shape in a Liquid-Filled Rotating Container Under Low Gravity," *Journal of Spacecraft and Rockets*, Vol. 25, No. 1, 1988, pp. 70–74.

[26]Harlow, F. H., and Welch, F. E., "N merical Calculation of Time-Dependent Viscous Incompressible Flow of Fluid with Free Surface," *Physics of Fluids*, Vol. 8, No. 11, 1965, pp. 2182–2189.

[27]Rubin, S. G., and Lin, T. C., "A Numerical Method for Three-Dimensional Viscous Flow: Application to the Hypersonic Leading Edge," *Journal of Computational Physics*, Vol. 9, No. 3, 1972, pp. 339–364.

[28]Salvadori, M. G., and Baron, M. L., *Numerical Methods in Engineering*, Prentice–Hall, Englewood Cliffs, NJ, 1961, pp. 37–252.

[29]Hageman, L. A., and Young, D. M., *Applied Iterative Methods*, Academic, New York, 1981, pp. 21–168.

[30]Young, D., "Iterative Methods for Solving Partial Difference Equations of Elliptical Type," *Transactions of the American Mathematical Society*, Vol. 76, No. 2, 1954, pp. 92–111.

[31]Patanker, S. V., *Numerical Heat Transfer and Fluid Flow*, Hemisphere–McGraw–Hill, New York, 1980, p. 197.

[32]Hung, R. J., Lee, C. C., and Leslie, F. W., "Effect of the Baffle on the Spacecraft Fluid Propellant Viscous Stress and Moment Fluctuations," *Transactions of the Japan Society for Aeronautical and Space Sciences*, Vol. 35, No. 2, 1993, pp. 187–207.

[33]Hung, R. J., and Lee, C. C., "Effect of a Baffle on Slosh Waves Excited by Gravity Gradient Acceleration in Microgravity," *Journal of Spacecraft and Rockets*, Vol. 31, No. 6, 1994, pp. 1107–1114.

[34]Hughes, P. C., *Spacecraft Attitude Dynamics*, Wiley, New York, 1986, p. 564.

[35]Greenwood, D. T., *Principles of Dynamics*, Prentice–Hall, Englewood Cliffs, NJ, 1965, p. 518.

[36]Hung, R. J., Long, Y. T., and Chi, Y. M., "Slosh Dynamics Coupled with Spacecraft Attitude Dynamics Part 2: Orbital Environment Application," *Journal of Spacecraft and Rockets*, Vol. 33, No. 4, 1996, pp. 582–593.

T. C. Lin
*Associate Editor*